ILASS-Americas 32nd Annual Conference on Liquid Atomization and Spray Systems, May 2022

Investigation of transcritical shock-droplet interaction using vapor-liquid equilibrium (VLE)-based CFD simulation

Hongyuan Zhang*, Suo Yang†
Department of Mechanical Engineering
University of Minnesota – Twin Cities
Minneapolis, MN 55455 USA

Abstract

To achieve high performance, the working pressure of liquid-fueled rocket engines, diesel engines, and gas turbines (based on deflagration or detonation) is continuously increasing, which could reach the thermodynamic critical pressure of the liquid fuel. For this reason, the studies of trans- and super-critical injection are getting more attention. However, most of the multiphase researches were mainly concentrated on single- or two-component systems, which cannot capture the multicomponent phase change in real high-pressure engines and gas turbines. The phase boundary, especially near the critical points, needs to be accurately determined to investigate the multicomponent effects in transcritical flow. This work used our previously developed thermodynamic model based on the vapor-liquid equilibrium (VLE) theory, which can predict the phase separation near the critical points. An in situ adaptive tabulation (ISAT) method was developed to accelerate the computation of the VLE model such that the expensive multicomponent VLE calculation can be cheap enough for CFD. The new thermodynamic model was integrated into OpenFOAM to build a VLE-based CFD solver. In this work, simulations are conducted using our new VLE-based CFD solver to reveal the phase change effects in transcritical flow. Specifically, shock-droplet interaction are investigated to reveal the shock-driven high pressure phase change.

*Ph.D Candidate.
†Richard & Barbara Nelson Assistant Professor, suoyang@umn.edu (Corresponding Author).

Introduction

The demand for high-performance combustors increases the chamber pressure continuously, making the working condition of some high-pressure combustors overlap with the supercritical region of fuel and/or oxidizer. The injection and mixing process is very different between subcritical and supercritical conditions [1, 2], which could affect the cold ignition in combustors. To understand the subcritical and supercritical mixing process, a simulation tool is needed. Since the behavior supercritical fluid can show significant difference from the ideal gas, the real-gas effect needs to be considered to capture correct behavior. In addition, transcritical and supercritical fluid behavior can be peculiar because of the considerable variation of thermophysical properties such as density and specific heat near the critical point. As a result, the Computational Fluid Dynamics (CFD) modeling of supercritical flows is very challenging. Since small changes in temperature and pressure can significantly affect a fluid's structure near the critical point, local properties are very important. Furthermore, a supercritical fluid lacks surface tension, which means the modeling transcritical flow needs to capture the surface tension change when the fluid goes across the phase boundary. This makes simulation of transcritical flow more challenging than supercritical flow.

The studies of transcritical and supercritical injection and mixing have attracted much interest in the past 30 years. However, most of them were mainly concentrated on the single-component system, whose critical point is a constant value. As long as the fluid exceeds its critical point, it goes into the supercritical state, and the classical "dense-fluid" approach is used with the assumption of a single-phase [3]. Since the real mixture critical pressure could be significantly higher than the critical pressure of each component [4], the accurate mixture critical point needs to be obtained.

Recently, some works focus on multicomponent transcritical flow simulation, capturing the phase separation at high pressure. Most works use the vapor-liquid equilibrium (VLE) theory to capture phase separation. Yao, et al. developed a fluids solver based on VLE to investigate the impact of diffusion models of a laminar counter-flow flame at trans and supercritical conditions [5]. In Ray's work, VLE theory is used to understand fuel droplets evaporation at high pressures [6]. A similar framework is also used in P. Tudisco's works to understand the effect of Lewis number [7].

However, all these works are limited to two-component transcritical flow simulation. The VLE solver brings a huge amount of computation cost, limiting the simulation of complex geometry and multicomponent flow. To reduce the computational cost, Tudisco, et al. interpolates the thermodynamic properties from cell-centers to cell-interfaces [8], but still can not accelerate the computation at cell-centers. Yi, et al. used a tabulation method to avoid computing of VLE model. However, the table size grows exponentially (table size M^N, M is the number of the grid in the table; N is the number of components). For a flow with four components, table size will need several Terabytes, making this method completely unsuitable for combustion and many other practical problems.

In this work, we coupled *In Situ* Adaptive Tabulation with the transcritical fluid solver to accelerate computation. The ISAT method constructs the table during the computation. It only stores the necessary data, which only requires a small amount of computer storage and achieves high computational speed [9]. The new solver with ISAT gained a great computational speed improvement. Then we conducted shock-droplet interaction simulation with 3 components to show the phase change effect under a high-pressure condition.

Numerical Modeling

Models of thermodynamic and transport properties

This study uses VLE solvers to capture the phase change and determine the multicomponent mixture's critical point in the transcritical flow. VLE describes the phase equilibrium between liquid and vapor phases. Solving the set of VLE equations gives the phase fraction and compositions in the two phases. If the gas mole fraction (i.e., the mole fraction of vapor phase) is equal to 1 or 0, then the system is in a purely gaseous or liquid phase, respectively. If the system falls into the two-phase region, the gas fraction will be between 0 and 1, and equilibrium between vapor and liquid will be observed. Suppose, at certain conditions, thermodynamic properties become identical between liquid and gas. In that case, it indicates the occurrence of a transcritical transition from a subcritical state to a supercritical state (which could be a liquid-like or gas-like state). The fluid solver that we implemented is coupled with isobaric and isenthalpic (PHn) flash solver[10]. PHn flash and almost all other VLE solvers are developed based on the TPn flash. Specifically, PHn flash solves the VLE equation set at given enthalpy (H) rather than temperature. The TPn flash is the most basic VLE solver, which solves the set of VLE equations at a given temperature (T), pressure (P), and mole fraction of

each component (n) in the system.

Isothermal and isobaric (TPn) flash:

VLE is governed by fugacity equality Eq. (1) and Rachford-Rice equation [11] Eq. (2), which is an additional constraint to the equilibrium solver as used in [12] and obtained from the conservation of each component.

$$f_{i,l}/f_{i,g} = 1 \tag{1}$$

$$\sum_{i=1}^{N} \left\{ z_i \left(1 - K_i\right) \Big/ \left[1 + \left(K_i - 1\right)\psi_g\right] \right\} = 0 \tag{2}$$

$$K_i = y_i/x_i \tag{3}$$

$$\sum_{i=1}^{N} x_i = \sum_{i=1}^{N} y_i = 1 \tag{4}$$

where $f_{i,p}$ is the fugacity of component i in phase p ($p = l$: liquid; $p = g$: gas), x_i is the mole fraction of component i in liquid phase, y_i is the mole fraction of component i in gas phase, z_i is the mole fraction of component i in the feed (i.e., the whole mixture including both gas phase and liquid phase), ψ_g is the gas mole fraction, K_i is the equilibrium constant of component i.

The real fluid properties are described using the Peng-Robinson equation of state (PR-EOS) [13] as:

$$P = \frac{RT}{V - b} - \frac{a}{V\left(V + b\right) + b\left(V - b\right)} \tag{5}$$

where P, R, T and V are pressure, gas constant, temperature, and specific volume respectively. For single-component fluid, the PR-EOS parameters are given by

$$a = 0.45724 \frac{R^2 T_c^2}{p_c} \hat{a}, \tag{6}$$

$$b = 0.07780 \frac{RT_c}{p_c}, \tag{7}$$

$$\hat{a} = \left(1 + \kappa\left(1 - \left(T_r\right)^{1/2}\right)\right)^2, \tag{8}$$

$$\kappa = 0.37464 + 1.54226\omega - 0.26992\omega^2 \tag{9}$$

where subscript "c" means critical value, subscript "r" means the reduced value (e.g., $T_r = T/T_c$), ω is acentric factor.

The mixture PR-EOS parameters are calculated from the corresponding single component coefficients a_i and b_i using the mixing rule [14]:

$$a = \sum_i \sum_j \chi_i \chi_j (1 - b_{ij}) \sqrt{a_i a_j} \tag{10}$$

$$b = \sum_i \chi_i b_i \tag{11}$$

where χ_i is the mole fraction of component i (for liquid, $\chi_i = x_i$; for gas phase, $\chi_i = y_i$), b_{ij} is a binary interaction parameter.

The liquid phase and the gas phase are described by two multicomponent PR-EOS, respectively. The specific volume of each phase, V_p, is solved from PR-EOS. The compressibility factor of each phase ($Z = PV/RT$) can also be obtained from this.

The fugacity formula of PR-EOS is shown below [15]:

$$\begin{aligned} f_i = & P\chi_i \exp\Bigg[\frac{B_i}{B_{mix}}(Z-1) - ln(Z - B_{mix}) \\ & - \frac{A_{mix}}{2\sqrt{2}B_{mix}}\left(\frac{2\sum_j x_j A_j}{A_{mix}} - \frac{B_i}{B_{mix}}\right) \\ & \times ln\left(\frac{Z + (1+\sqrt{2})B_{mix}}{Z + (1-\sqrt{2})B_{mix}}\right)\Bigg] \end{aligned} \tag{12}$$

where χ_i is the mole fraction of component i (for liquid, $\chi_i = x_i$; for gas phase, $\chi_i = y_i$),

$$A_i = \frac{a_i p}{R^2 T^2}, \tag{13}$$

$$B_i = \frac{b_i p}{RT}, \tag{14}$$

$$A_{mix} = \sum_i \sum_j x_i x_j (1 - b_{ij}) \sqrt{A_i A_j}, \tag{15}$$

$$B_{mix} = \sum_i x_i B_i \tag{16}$$

The equation set Eq. (1-16) is solved based on Newton iteration method. The flow chart of the TPn flash is shown in Fig. 1. The initial guess is obtained using Wilson Equation [16]:

$$K_i = e^{5.373(1+\omega_i)(1-1/T_{r,i})}/P_{r,i} \tag{17}$$

where ω_i is the acentric factor of component i; $T_{r,i}$ and $P_{r,i}$ are the reduced temperature and reduced pressure of component i, respectively. Then, solving Rachford-Rice equation (i.e., Eq. 2) using Newton iteration method to get ψ_g. x_i and y_i can be obtained from Eqs. (3) and (4). The next step is to evaluate fugacity using the Eq. (12-16), and examine whether fugacity equilibrium (i.e., $f_{i,l} = f_{i,g}$) has been reached. If not, update K_i by $K_i = K_i \times f_{i,l}/f_{i,g}$ and go back to solve Rachford-Rice equation. When the error is less than a tolerance (i.e., the Newton iteration is converged), the solver will break the loop and output the solution.

Isobaric and Isenthalpic (PHn) flash:

In this work, the fluid solver uses the Double-Flux (DF) approach [17, 18] with central-upwind scheme [19], which directly updates pressure, enthalpy, and mass fraction of every component from

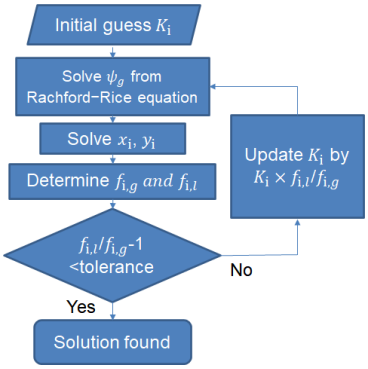

Figure 1. Flow chart of the TPn flash solver.

the fluid governing equation and the DF model. The equilibrium temperature T_{eq} is determined using PHn flash to evaluate other thermodynamic and transport properties. The corresponding objective function is expressed as

$$F_h = (h^* - h)/h^* \tag{18}$$

where h^* is the specific mixture enthalpy obtained from the fluid solver. The enthalpy of each phase p is calculated as

$$h_p(T,P) = h_{p,ideal}(T,p) + h_{p,dep}(T,p) \tag{19}$$

where h_{ideal} is the enthalpy of component i in ideal gas state, which is evaluated by JANAF polynomials; and h_{dep} is the departure enthalpy, calculated as:

$$h_{p,dep}(T,P) = RT(Z_p - 1) + \frac{T\frac{da_p}{dT} - a_p}{2\sqrt{2}b_p} ln \frac{Z_p + (1+\sqrt{2})B_{p,mix}}{Z_p + (1-\sqrt{2})B_{p,mix}} \tag{20}$$

where a_p, b_p and $B_{p,mix}$ are PR-EOS parameters of phase p defined in Eq. (10,11,16).

The enthalpy of two-phase mixture is calculated as

$$h = \psi_g h_g + (1-\psi_g) h_l \tag{21}$$

The equation is solved by the Newton iteration method. Equilibrium temperature T_{eq} is updated in PHn flash iteratively as

$$T_n = T_{n-1} + (h^* - h(T_{n-1}, P)) \Big/ C_{p,mix}(T_{n-1}, P) \tag{22}$$

$$C_{p,mix} = \frac{h(T+\Delta T, P) - h(T,P)}{\Delta T} \tag{23}$$

Transport properties:

The dense fluid formula [20] is used to evaluate the dynamic viscosity and thermal conductivity under transcritical conditions. This method gives accurate estimations of viscosity and thermal conductivity of polar, non-polar and associating pure fluids and mixtures. Its dynamic viscosity and thermal conductivity have a similar formula:

$$\lambda = \lambda_0 \lambda^* + \lambda_p \tag{24}$$

where λ represents dynamic viscosity or thermal conductivity. λ_0 is the gas property at low pressures. λ^* and λ_p are high-pressure corrections. At high pressures, λ_p is the major contributing term comparing to $\lambda_0\lambda^*$. On the other hand, at low pressures, λ^* is approaching unity, and the λ_p term is negligible such that Eq. 24 reduces to λ_0. Hence, the transition between subcritical and supercritical is smoothly described by the model.

For mas diffusivity we used mixture-averaged mass diffusion model. The mass diffusion coefficient of specie i, D_i, which is defined by [21],

$$D_i = \frac{1 - Y_i}{\sum_{j \neq i}^{N} X_j / D_{j,i}} \tag{25}$$

where Y_i and X_i are the mass and mole fractions of i-th species, respectively; $D_{i,j}$ is the binary diffusion coefficient, which is evaluated by Fuller's model [22] with Takahashi's correction [23].

In Situ Adaptive Tabulation (ISAT)

In situ adaptive tabulation method is introduced by Pope [9] to reduce the computational cost of detailed chemistry calculations. Compared to the traditional tabulation methods, which generate a table before computation, ISAT dynamically constructs a table during the computation, which enables us to store necessary records to reduce the table size. Although ISAT still needs to calculate the target function, most queries can be directly retrieved by linear approximation. In addition, ISAT does not only balance time and space cost but also provides good error control. Hence, it is a good choice to accelerate the PHn flash solver.

The fluid solver directly updates pressure P, enthalpy h, and mass mole fraction of every component Y_m from the governing equation, and require thermodynamic model to evaluate temperature T, and gas mole fraction ψ_g and speed of sound c. (T,ψ_g) can be solved by PHn flash solver, c is obtained from analytical approach [24]. The relation between the given condition and solution of PHn flash solver can be denote as a function,

$$\boldsymbol{y} = \boldsymbol{F}(\boldsymbol{x}), \mathbf{x} = (\mathbf{Y}, P, h), \mathbf{y} = (T, \phi, \psi_g)$$

For every record in the table, it contains $(\mathbf{x}_0, \mathbf{y}_0, \frac{\partial \mathbf{F}}{\partial \mathbf{x}}\big|_{\mathbf{x}_0}, \mathbf{M})$

The gradient, $\frac{\partial \mathbf{F}}{\partial \mathbf{x}}\big|_{\mathbf{x}_0}$, is evaluated using analytical framework derived in [24] and used for local linear approximation. Due to the derivative of c require more complex formula. For simplicity, the derivative of c is set as zero.

$$\mathbf{y}_{linear} = \mathbf{y}_0 + \frac{\partial \mathbf{F}}{\partial \mathbf{x}}\bigg|_{\mathbf{x}_0} \cdot (\mathbf{x} - \mathbf{x}_0)$$

The matrix $\mathbf{M}$ is used to define the region of accuracy, in which the local error ϵ does not exceed the tolerance ϵ_{tol}. The region of accuracy is defined by inequality

$$(\mathbf{x} - \mathbf{x}_0)^T \mathbf{M} (\mathbf{x} - \mathbf{x}_0) \leq 1$$

The point satisfying this inequality is a hyper-ellipsoid. So, the region of accuracy is also called ellipsoid of accuracy (EOA).

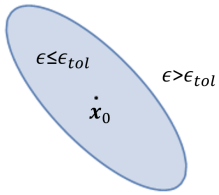

Figure 2. Sketch of region of accuracy

For the initial setting, the linear term is considered as the error. So, the initial $\mathbf{M}$ can be set as

$$\mathbf{M} = \left(\frac{\partial \mathbf{F}}{\partial \mathbf{x}}\bigg|_{\mathbf{x}_0}\right)^T \left(\frac{\partial \mathbf{F}}{\partial \mathbf{x}}\bigg|_{\mathbf{x}_0}\right) / \epsilon_{tol}^2$$

.

For the first query, a new record is calculated and added to the table. For subsequent queries $(\mathbf{x}_{new})$, the closest record $(\mathbf{x}_0, \mathbf{y}_0, \frac{\partial \mathbf{F}}{\partial \mathbf{x}}\big|_{\mathbf{x}_0}, \mathbf{M})$ is find out.

(1). **Retrieve**. If $\mathbf{x}_{new}$ is in the EOA of the record, then the linear approximation, $\mathbf{y}_{linear}$, is returned.

(2). **Growth**. If retrieve failed, then $\mathbf{y}_{new} = \mathbf{F}(\mathbf{x}_{new})$ is calculated. If $|\mathbf{y}_{new} - \mathbf{y}_{linear}| \leq \epsilon_{tol}$, the EOA is grown. The new EOA is the smallest ellipsoid covering old EOA and $\mathbf{x}_{new}$. $\mathbf{y}_{new}$ is returned.

(3). **Addition**. If growth also failed, then a new record is added to the table, and $\mathbf{y}_{new}$ is returned.

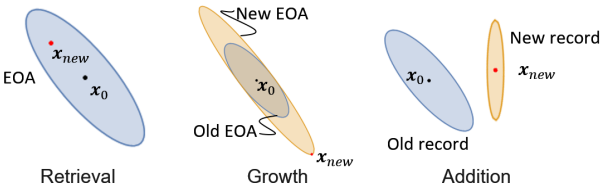

Figure 3. Sketch showing the algorithm of ISAT method

CFD simulation framework

In this investigation, a transcritical multiphase CFD solver is developed by coupling a CFD solver with the TPn flash VLE solver. The CFD solver is based on multicomponent transport equations, including the continuity equation, mixture momentum equations, mixture specific internal enthalpy equation, and balance equations for distinct components in the mixture as follows:

$$\frac{\partial \rho}{\partial t} + \frac{\partial \rho u_i}{\partial x_i} = 0 \tag{26}$$

$$\frac{\partial \rho u_i}{\partial t} + \frac{\partial \rho u_i u_j}{\partial x_j} = \frac{\partial P}{\partial x_i} + \frac{\partial \tau_{ij}}{\partial x_j} \tag{27}$$

$$\frac{\partial \rho (e + K)}{\partial t} + \frac{\partial \rho u_i (e + K) + u_i P}{\partial x_i} = -\frac{\partial q_i}{\partial x_i} + \frac{\partial \tau_{ij} u_j}{\partial x_i} \tag{28}$$

$$\frac{\partial \rho Y_m}{\partial t} + \frac{\partial \rho Y_m u_j}{\partial x_i} = \frac{\partial}{\partial x_j}\left(\rho D \sum_m h_m \frac{\partial Y_m}{\partial x_j}\right) \tag{29}$$

where ρ and e are mixture density and internal energy, respectively, and Y_m is mass fraction of component m.

The CFD solver is developed based on the central-upwind scheme [19]. The Double-Flux (DF) approach [17, 18] is used to mitigate the pressure fluctuations caused by real gas effect. At each time step, rho, u, and Y_i are updated using central-upwind scheme. Then, the DF model is used to update e and p. After that, T, ψ_g, c are updated using ISAT VLE model. This process is shown in Fig. 4.

Result and Analysis

Fluid simulation: 2D shock-droplet interaction

A test case is conducted on a two-dimensional domain and simulates the interaction of a shock with a droplet. The schematic of the 2D shock-droplet interaction is shown in Fig. 5. This test case is to study the multicomponent VLE effect as the thermodynamic state is suddenly changed by the shock. The simulations use a squared shape domain with side $L = 1m$ and the uniform grid is discretized using

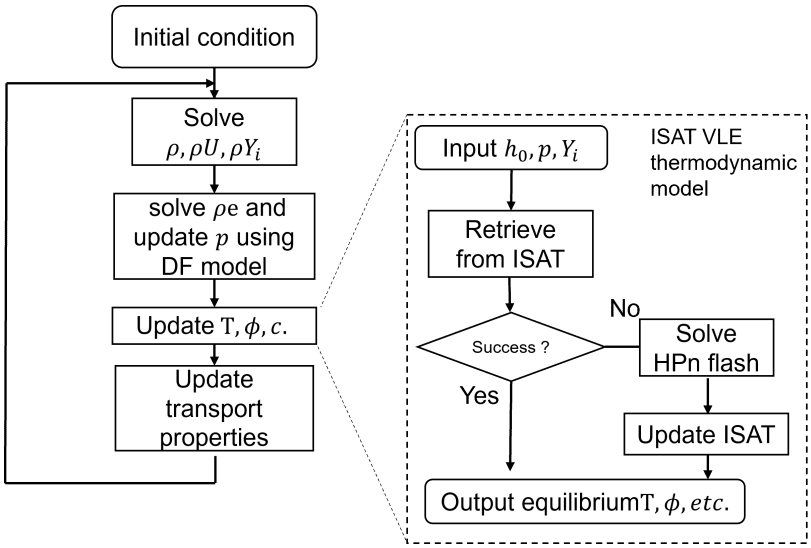

Figure 4. Flow chart of the VLE-based CFD solver.

128×128 grid points. The initial droplet is placed at the center of the square with a diameter $d = L/4$. The droplet is composed of C_6H_{14}. The surrounding environment is filled with to N_2 and H_2O (5% H_2O by mass). A high pressure region ($l = 0.2m$) is set to generate a shock wave.

The initial state of the low pressure region is set to $p = 20$ MPa, $T = 311$ K, $u = v = 0$, which is a VLE condition for this mixture. On the other hand, the high pressure region is set to $p = 240$ MPa, $T = 311$ K, $u = v = 0$. Post shock conditions are $p = 38$ MPa, $u = 198$ m/s and $T = 459$ K. This condition is expected to push the mixture into supercritical region. Analysis is conducted by taking four instantaneous snapshots corresponding to four different time instants: $t_1 = 19.3\ \mu s$, $t_2 = 31.0\ \mu s$, $t_=$42.7 μs and $t_4 = 54.4\ \mu s$, roughly corresponding to an interaction of the shock with 25, 50, 75 and 100 percent of the bubble surface, Fig. 5.

The simulation is run serially on a PC equipped with an Intel Core i7-8700K CPU. The running time of the simulation with ISAT is about 3 times faster than the one without ISAT model.

The time sequence contour plots of the phase fraction, pressure and temperature in Fig. 6. The plots show that when shock-droplet interaction start, a reflect wave and a incident wave form. The reflection wave generates a high temperature and high pressure region in front of the droplets, which which evaporate the liquid water in the region. The incident wave is weaker than reflection wave. In addition, the surface of the droplet is under VLE condition. Due to the high pressure and temperature caused by shock, the state of interface enters the supercritical state (the vapor fraction reaches 1). When the shock pass through the droplets, the droplet is squeezed horizontally, but no optimization happens. The reason might be: the surface tension is one major mechanism of atomization, which is not captured by current model. The density outside of the droplets at four time instants are show in Fig 7. The reflection wave can be observed on the plots. Compared to the VLE results, the result without VLE model shows lower density in reflection wave.

Conclusion

We implemented a vapor-liquid equilibrium (VLE) solver (PHn flash) and coupled PHn flash solver with a computational fluid dynamics (CFD) solver using central upwind scheme and Double-flux method to capture the mixing and phase separation processes of mixtures. The ISAT method speed up the simulation by 3 times. A shock-droplet interaction simulation is conducted. The results the capture the droplet entering the supercritical state after shock passes through. The evaporation of liquid water in surrounding caused by reflection wave is also captured.

Acknowledgments

S. Yang gratefully acknowledges the grant support from NSF CBET 2023932. H. Zhang gratefully acknowledges the support from the Frontera Computational Science Fellowship.

References

[1] B Chehroudi, D Talley, and E Coy. *37th Aerospace Sciences Meeting and Exhibit*, p. 206,

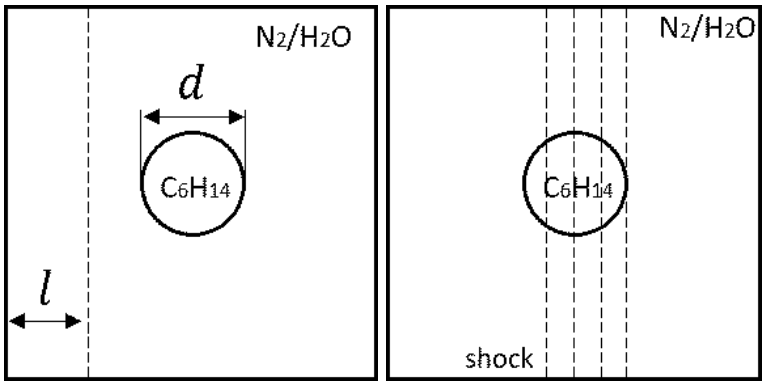

Figure 5. Schematic of the 2D shock-droplet interaction. Left: relevant dimensions. Right: shock position at which data is analyzed

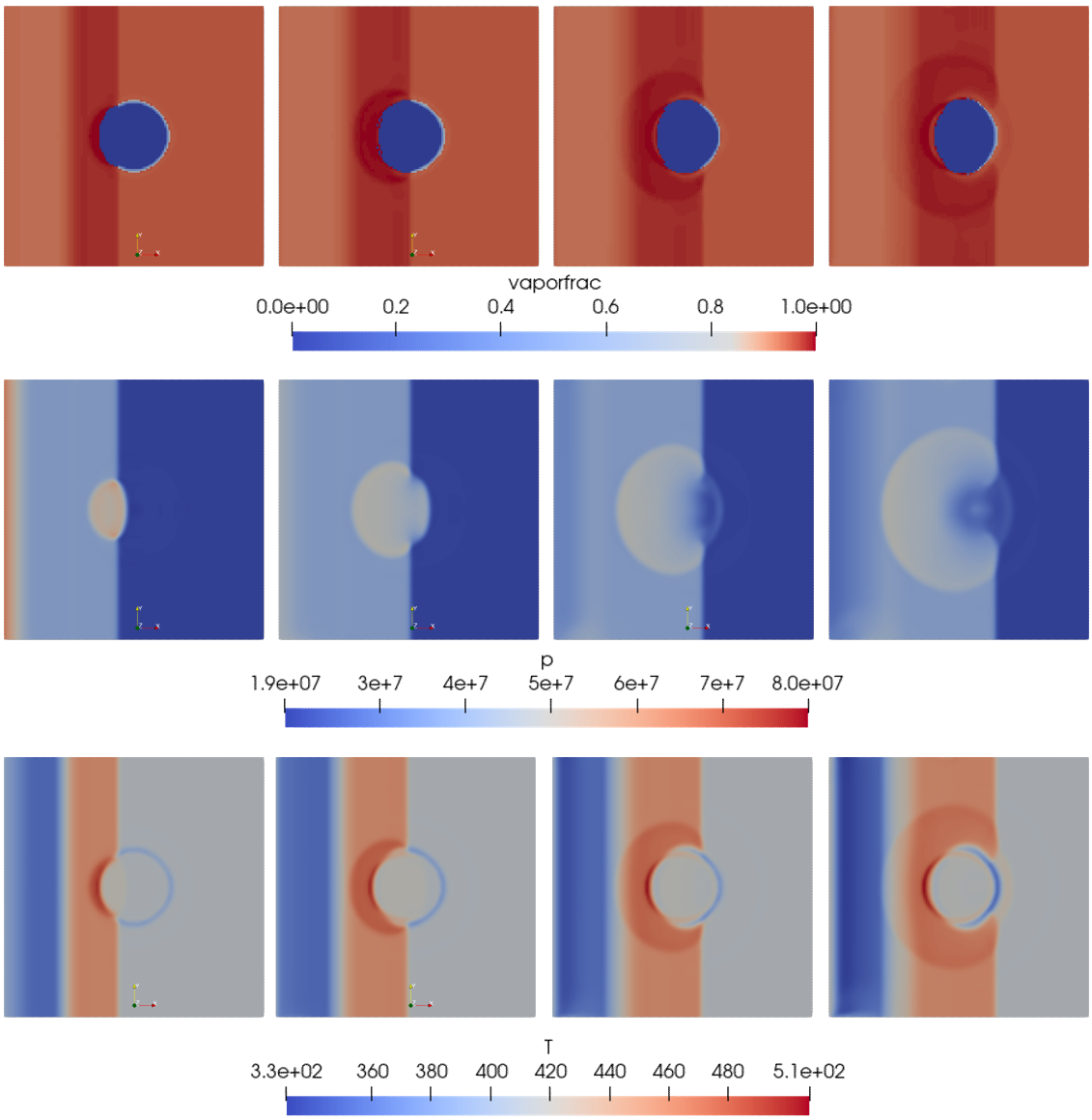

Figure 6. Time sequence contour snapshots of phase fraction, pressure and temperature.

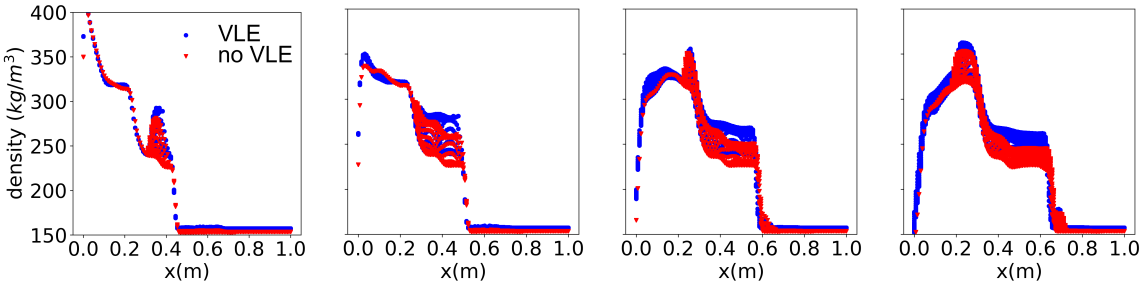

Figure 7. Density plots of four time instants outside of the droplets

1999.

[2] W Mayer and Joshua J Smith. *Liquid Rocket Thrust Chambers: Aspect of Modeling, Analysis, and Design, Progress in Astronautics and Aeronautics*, 200:339–368, 2004.

[3] Vigor Yang. *Proceedings of the Combustion Institute*, 28(1):925–942, 2000.

[4] PH Van Konynenburg and RL Scott. *Philosophical Transactions of the Royal Society of London. Series A, Mathematical and Physical Sciences*, 298(1442):495–540, 1980.

[5] Matthew X Yao, Jean-Pierre Hickey, Peter C Ma, and Matthias Ihme. *Combustion and Flame*, 210:302–314, 2019.

[6] Saroj Ray, Vasudevan Raghavan, and George Gogos. *International Journal of Multiphase Flow*, 111:294–309, 2019.

[7] P Tudisco and S Menon. *Physics of Fluids*, 32(11):112111, 2020.

[8] Principio Tudisco and Suresh Menon. *Flow, Turbulence and Combustion*, 104(2):693–724, 2020.

[9] Stephen B Pope. *Combustion Theory and Modelling*, 1(1):41–63, 1997.

[10] Michael L Michelsen. *Fluid phase equilibria*, 33(1-2):13–27, 1987.

[11] HH Rachford Jr, JD Rice, et al. *Journal of Petroleum Technology*, 4(10):19–3, 1952.

[12] Sanjoy Saha and John J Carroll. *Fluid phase equilibria*, 138(1-2):23–41, 1997.

[13] Ding-Yu Peng and Donald B Robinson. *Industrial & Engineering Chemistry Fundamentals*, 15(1):59–64, 1976.

[14] Robert C Reid, John M Prausnitz, and Thomas K Sherwood. *The Properties of Liquids and Gases.(Stichworte Teil 2)*. McGraw-Hill, 1977.

[15] Ping Yi, Songzhi Yang, Chaouki Habchi, and Rafael Lugo. *Physics of Fluids*, 31(2):026102, 2019.

[16] Grant M Wilson. *Journal of the American Chemical Society*, 86(2):127–130, 1964.

[17] Rémi Abgrall and Smadar Karni. *Journal of computational physics*, 169(2):594–623, 2001.

[18] G Billet and R Abgrall. *Computers & fluids*, 32(10):1473–1495, 2003.

[19] Alexander Kurganov, Sebastian Noelle, and Guergana Petrova. *SIAM Journal on Scientific Computing*, 23(3):707–740, 2001.

[20] Ting Horng Chung, Mohammad Ajlan, Lloyd L Lee, and Kenneth E Starling. *Industrial & engineering chemistry research*, 27(4):671–679, 1988.

[21] Robert J Kee, Fran M Rupley, Ellen Meeks, and James A Miller. Chemkin-iii: A fortran chemical kinetics package for the analysis of gas-phase chemical and plasma kinetics. Technical report, Sandia National Lab.(SNL-CA), Livermore, CA (United States), 1996.

[22] Edward N Fuller, Paul D Schettler, and J Calvin Giddings. *Industrial & Engineering Chemistry*, 58(5):18–27, 1966.

[23] Shinji Takahashi. *Journal of Chemical Engineering of Japan*, 7(6):417–420, 1975.

[24] P Tudisco and S Menon. *The Journal of Supercritical Fluids*, 164:104929, 2020.